Dynamical nuclear polarization for dissipation-induced entanglement in NV centers

Shishir Khandelwal,[1] Shashwat Kumar,[2] Nicolas Palazzo,[2] Géraldine Haack,[1] and Mayeul Chipaux[2,*]
[1]*Département de Physique Appliquée, Université de Genève, 1211 Genève, Switzerland*
[2]*Institute of Physics, École Polytechnique Fédérale de Lausanne (EPFL), 1015 Lausanne, Switzerland*

(Received 12 July 2023; revised 8 October 2023; accepted 9 October 2023; published 13 November 2023)

We propose a practical implementation of a two-qubit entanglement engine which denotes a scheme to generate quantum correlations through purely dissipative processes. On a diamond platform, the electron spin transitions of two nitrogen-vacancy (NV) centers play the role of artificial atoms (qubits), interacting through a dipole-dipole Hamiltonian. The surrounding carbon-13 nuclear spins act as spin baths playing the role of thermal reservoirs at well-defined temperatures and exchanging heat through the NV center qubits. In our scheme, a key challenge is therefore to create a temperature gradient between two spin baths, for which we propose to exploit the recent progress in dynamical nuclear polarization, combined with microscopy superresolution methods. We discuss how these techniques should allow us to initialize such a long lasting out-of-equilibrium polarization situation between them, effectively leading to suitable conditions to run the entanglement engine successfully. Within a quantum master equation approach, we make theoretical predictions using state-of-the-art values for experimental parameters. We obtain promising values for the concurrence, reaching theoretical maxima.

DOI: 10.1103/PhysRevB.108.174418

I. INTRODUCTION

The generation of quantum entanglement is a crucial task for quantum information processing. Typically, this requires performing logical two-qubit unitary operations and limiting the quantum systems' interaction with their environment

These implementations require isolating the quantum systems from their environment, and platform-dependent techniques have been developed to achieve that, for superconducting circuits [1] and trapped ions [2], for instance. However, avoiding all possible sorts of uncontrolled dissipation processes is impossible. In this context, natural questions arises. Is it possible to exploit dissipation with thermal environments to create quantum resources? And how could this be implemented? In recent years, those questions have triggered a number of theoretical works, leading to proposals for realizing thermal machines generating quantum correlations [3–9]. It has also been demonstrated that the generated entanglement can be useful for performing nonclassical operations [10,11]. However, experimental demonstrations of these ideas are still lacking. In this work, we propose an experimental implementation of a two-qubit entanglement engine based on diamond NV centers.

NV centers, which are compounds of a nitrogen substitution (N) and a vacancy (V) in two adjacent sites of the diamond lattice, are recognized as one of the most promising platforms for quantum technologies. As first demonstrated in 1997 [12], they possess the features of an optically detected magnetic resonance (ODMR) system [13]. This means that their electron-spin, coherently controlled with microwaves, can be initialized and read out with optical means. This is typically performed with standard microwaves and visible range photoluminescence microscopy equipment [14]. NV centers can also be addressed with superresolution methods such as ground state depletion (GSD) [15] or stimulated emission depletion (STED) [16] with resolution down to 6 nm [17]. Combined with remarkable room-temperature quantum properties [18], these qualities make NV centers particularly successful for quantum sensing applications [19–21], allowing for very versatile experimental conditions such as high pressure [22] or high temperature [23] conditions or within biological environments [24].

NV centers also constitute a promising platform for quantum information processing [25,26]. Their fine and hyperfine structure with surrounding electron or nuclear spins gives them numerous controllable quantum degrees of freedom. Notably, NV centers can be exploited to control and entangle the dark electron and nuclear spins of nearby P1 centers (corresponding to a nitrogen substitution) [27]. They are also often used as a quantum bus to control multiple surrounding carbon-13 (^{13}C) nuclear spins operating as quantum memories [28]. In parallel, dynamical nuclear polarization (DNP) techniques [29–32] have been developed to control the state of nuclear spins which are near the NV centers. These nuclear spins can be located in the bulk or at the surface of the diamond, and they can correspond to different elements (^{13}C, ^{19}F, or ^{1}H). These techniques were primarily developed towards hyperpolarized nuclear magnetic resonance (NMR) applications [33]. From the perspective of open quantum systems, they constitute a path to realize effective spin baths with specific properties that can be controlled through the NV centers.

In this work, we exploit recent developments in the field of NV centers to propose an experimental scheme for a thermal

*Corresponding author: mayeul.chipaux@epfl.ch

machine to produce entanglement between the electron spins of two NV centers. Towards this goal, we put forward DNP techniques to engineer two effective spin baths characterized by distinct polarizations. More precisely, we detail two regimes accessible with DNP techniques, namely the cross-relaxation (CR) regime [29] and the low-field Hartmann-Hahn (HH) regime [34], in which the "NOVEL" method is derived [30,31] schemes belong, for instance. The CR regime, although simpler conceptually as it only requires the two quantum systems to be at resonance, is experimentally challenging. In our scheme, as detailed below, this resonant condition can only be achieved with demanding microscopic superresolution techniques such as GSD and STED mentioned above. On the contrary, the HH regime makes it possible to set the desired resonance in the qubit rotating frames by continuously driving them in their equatorial plane. This allows for greater flexibility, making it particularly attractive for manipulating NV centers for various applications. In the present proposal, we discuss both regimes.

The article is organized as follows. In Sec. II, we briefly recall the basic ingredients of an entanglement engine to achieve dissipation-induced entanglement between two artificial atoms. In Sec. III, we propose the electron spin of an NV center to play the role of an artificial atom, elaborating upon the various energy scales involved and the conditions to be satisfied to have steady-state entanglement between the electron spins. In Sec. IV A, we discuss how these electron spins can be made to interact with their surrounding ^{13}C nuclear spin bath. In Sec. V, we tackle the main challenges of this proposal, namely the realization of two thermal environments biased in temperature. In Secs. III–V, we discuss the specifics of CR- and HH-regime operations. Section VI presents our predictions for the presence of entanglement for the first configuration.

II. THEORETICAL MODEL

A minimal model to investigate entanglement generation from dissipation is made of two interacting artificial atoms (qubits), each of them being tunnel-coupled to a thermal environment. These environments are assumed to be independent from one another, and well-defined by their respective temperature and chemical potential through their Fermi distribution. When subject to a bias in temperature, a heat current flows between the two environments through the system. If the qubits are interacting through a flip-flop type Hamiltonian (see below), this heat current has been demonstrated to sustain the presence of entanglement in the steady-state regime [3,6,35], and proposals were developed for semiconducting and superconducting platforms [8,9]. We now briefly recall the Hamiltonian of the two interacting qubits in this model, as well as the master equation that will be used to investigate the dynamics of this entanglement engine.

The Hamiltonian of the two qubits is given by

$$H_S = \varepsilon_L \sigma_L^+ \sigma_L^- \otimes \mathbb{1}_R + \mathbb{1}_L \otimes \varepsilon_R \sigma_R^+ \sigma_R^- + g(\sigma_L^+ \otimes \sigma_R^- + \sigma_L^- \otimes \sigma_R^+), \quad (1)$$

where ε_α ($\alpha = $ L,R) are the energies of the left (L) and right (R) qubits, and g is the strength of the interqubit coupling. The raising and lowering operators for qubit α are, respectively, σ_α^+ and σ_α^-. For a two-qubit device, it has been shown that a flip-flop-type interaction Hamiltonian is suitable for entanglement generation [3,6]. The qubits are distinctly coupled to two fermionic reservoirs (the choice is suitable for the NV-center platform, as we explain below). Assuming Markovian dynamics and weak system-reservoir couplings, the dissipative dynamics of the qubits can be described by a Lindblad master equation. Furthermore, if the interaction g is small in comparison to ε_α, the following local master equation is consistent [36]:

$$\dot{\rho}(t) = -i[H_S, \rho(t)] + \sum_{\alpha \in \{L,R\}} \gamma_\alpha^+ \mathcal{D}[\sigma_\alpha^+]\rho(t) + \gamma_\alpha^- \mathcal{D}[\sigma_\alpha^-]\rho(t), \quad (2)$$

with the dissipators defined as $\mathcal{D}[A]\rho(t) \coloneqq A\rho(t)A^\dagger - \{A^\dagger A, \rho(t)\}/2$, and $\sigma_\alpha^\pm$ the raising and lowering operators.

In the case of fermionic baths, the Fermi distribution $n_F(\varepsilon_\alpha, T_\alpha)$ characterizing the environment of qubit α is evaluated at the qubit's energy ε_α and temperature T_α. The total coupling rates are the product of the bare rate Γ_α (which depends on the microscopic details of the platform) and of the occupation probability of the environment [36],

$$\gamma_\alpha^+ = \Gamma_\alpha \, n_F(\varepsilon_\alpha, T_\alpha),$$
$$\gamma_\alpha^- = \Gamma_\alpha [1 - n_F(\varepsilon_\alpha, T_\alpha)]. \quad (3)$$

A temperature gradient between the two baths, $T_L \neq T_R$, induces a heat current flowing through the system. It was shown in [3,6] that, above a certain threshold for the heat current, entanglement between the two qubits is present in the steady state, but also in the transient regime. In the following sections, we discuss how to realize this model on a NV-center platform, first showing how the coupling between the NV-center qubits can be realized, and then showing how an effective temperature (polarization) gradient between the qubits can be created.

III. REALIZATION OF THE SYSTEM HAMILTONIAN

A. The diamond NV center

The NV center's optical ground state is a spin triplet. Interestingly, it can be initialized by an off-resonance optical green pump (e.g., 520 or 532 nm) and read out through its red photoluminescence (from 600 to 800 nm). Figure 1 represents the NV centers, their simplified energy diagram, and a typical experimental setup for their study. With $\vec{S} = \{S_x, S_y, S_z\}$ the NV-center electron spin and m_S the associated quantum number, the NV center ground-state Hamiltonian in a magnetic field $\vec{B}$ can be written as

$$H_{NV} = DS_z^2 + \gamma_e \vec{B} \cdot \vec{S} + H_N + H_T, \quad (4)$$

where the constant $D = 2\pi \times 2.87\,\text{GHz}$ is the zero field splitting (ZFS) and $\gamma_e = g\mu_B/\hbar = 2\pi \times 28.0\,\text{GHz}\,\text{T}^{-1}$ is the electron spin gyromagnetic ratio. H_N and H_T describe the hyperfine interaction of the NV center electron spin $\vec{S}$ with the nitrogen atom (^{14}N or ^{15}N) and the surrounding ^{13}C (see Sec. IV A).

We denote as $B_\parallel$ and $B_\perp$ the longitudinal and the transverse components of the magnetic field with respect to the NV center quantization axis N-V joining the nitrogen to the

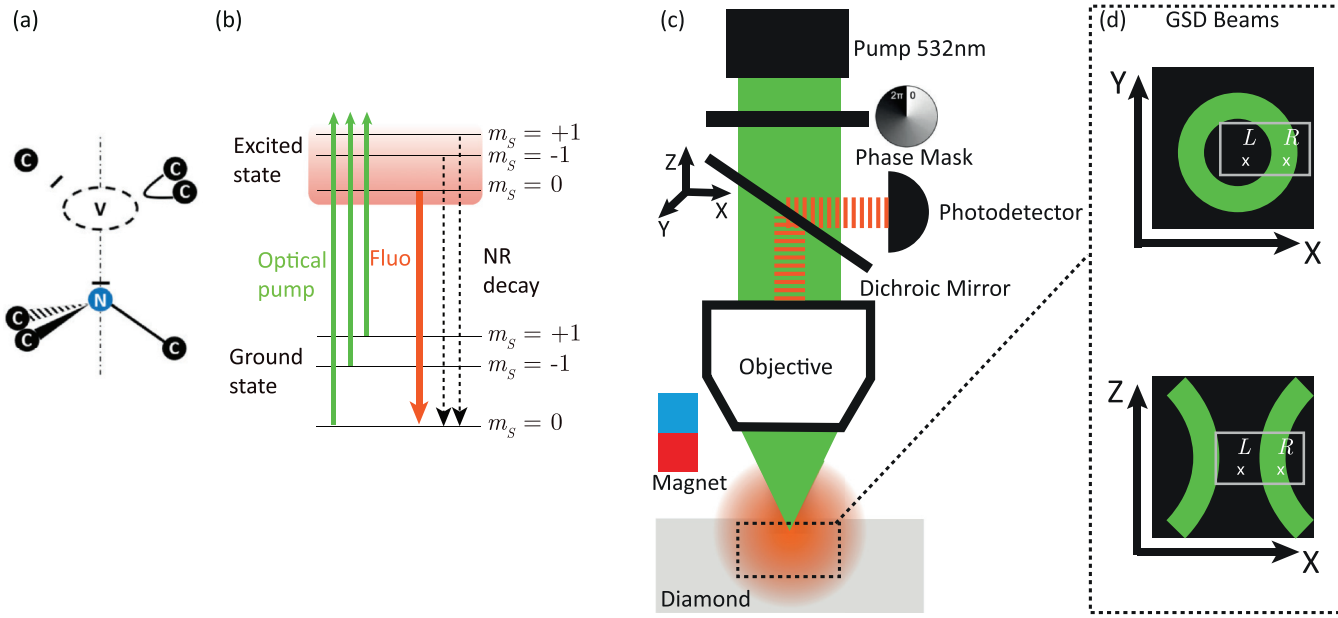

FIG. 1. (a) Sketch of a NV center in diamond with the nitrogen substitution (N) next to the vacancy (V) in the lattice made of carbon (C). The electrons are shown in the Natta projection for three-dimensional aspects. (b) NV center simplified energy diagram. The NV center is pumped by a green laser (typically at 520 or 532 nm) and emits a red broadband photoluminescence whose zero-phonon line is at 637 nm. A spin-dependent nonradiative decay path (dashed lines) enables its ODMR properties (e.g., optical initialization and readout). (c) Representation of an experimental setup for targeting the centers embedding ground state depletion superresolution capabilities required in the CR regime (configuration no. 1).

vacancy. The eigenenergies of the NV center corresponding to the spin states $|m_s = \pm 1\rangle$ can be controlled through $B_\parallel$ according to the following equation [37,38], up to first order in $B_\perp$ (see hereafter): $\varepsilon_\pm(B_\parallel) = D \pm \gamma_e B_\parallel$. In the following, we consider the energy transition from the ground state to the lowest excited state $|m_s = -1\rangle$ as the qubit transition,

$$\varepsilon_{\mathrm{L,R}} \equiv \varepsilon_- = D - \gamma_e B_\parallel. \tag{5}$$

To realize the Hamiltonian of Eq. (1), and the system evolution according to Eq. (2), it is essential that the two electronic spins are resonant not only with each other, but also with the nuclear spins of the surrounding ^{13}C. Under the assumption of a parallel magnetic field only, the energy of the nuclear spins of the ^{13}C is simply given by

$$\varepsilon_n = \gamma_n B_\parallel. \tag{6}$$

Now, there are two regimes, CR and HH, to implement this resonant condition between the two qubits themselves and the nuclear spins.

B. Cross-relaxation regime

In the cross-relaxation (CR) regime, one requires the condition $\varepsilon_{L,R} = \varepsilon_n$ to be satisfied, with $\varepsilon_{L,R}$ and ε_n given by Eqs. (5) and (6). This is achieved with the modulus of the magnetic field to be close to the ground state level anticrossing (GSLAC) condition:

$$\varepsilon_{L,R} = D - \gamma_e B_\parallel = \gamma_n B_\parallel \tag{7}$$

$$\Leftrightarrow B_\parallel := B_{CR} = D/(\gamma_e + \gamma_n) \sim 102\ \mathrm{mT}. \tag{8}$$

For estimating B_{CR}, we have assumed $\gamma_n \ll \gamma_e$, valid for any nuclear spin with respect to any electronic spin. The label *CR* in the magnetic field refers to the energy-resonance condition, known as the cross-relaxation regime [39,40].

The energy-resonance regime must be reached while preserving the NV centers' quantization axes and their ODMR properties [41]. This imposes that the applied magnetic field must be well aligned with the quantization axis $(N - V)$ of the two qubits, hence $B_\perp \approx 0$ as in Eq. (5). This also implies that the two NV centers are along the same crystallographic orientation, aligned with the magnetic field. The experimental scheme corresponding to operating in the CR regime is illustrated in Fig. 2 (hereafter also configuration no. 1).

C. Hartmann-Hahn regime

An alternative to the cross-relaxation regime is provided by low-field DNP methods [30–32]. These methods consist in driving the qubits continuously to maintain them in their energy eigenbasis (dressed states), characterized by their energies $\varepsilon^1_{L,R} = \gamma_e B^1_{L,R}$. This is done by driving each qubit individually with a microwave magnetic field $B^1_{L,R}\cos(\omega_{\mathrm{MW}} t)$ at resonance with the qubit, $\omega_{\mathrm{MW}} = \varepsilon_{L,R}/\gamma_e$. The Hartmann-Hahn (HH) regime [34] is then satisfied by adjusting these eigenenergies to the energy of the nuclear spins,

$$\varepsilon^1_{\mathrm{L,R}} = \varepsilon_n \Leftrightarrow B^1_{\mathrm{L,R}} = \frac{\gamma_n}{\gamma_e} B_\parallel. \tag{9}$$

The corresponding experimental configuration, denoted no. 2, is shown in Fig. 3. It is similar to the recent DNP experiments [30,32], where they have used the so-called NOVEL sequence derived from the initial Hartmann-Hahn method [34]. As

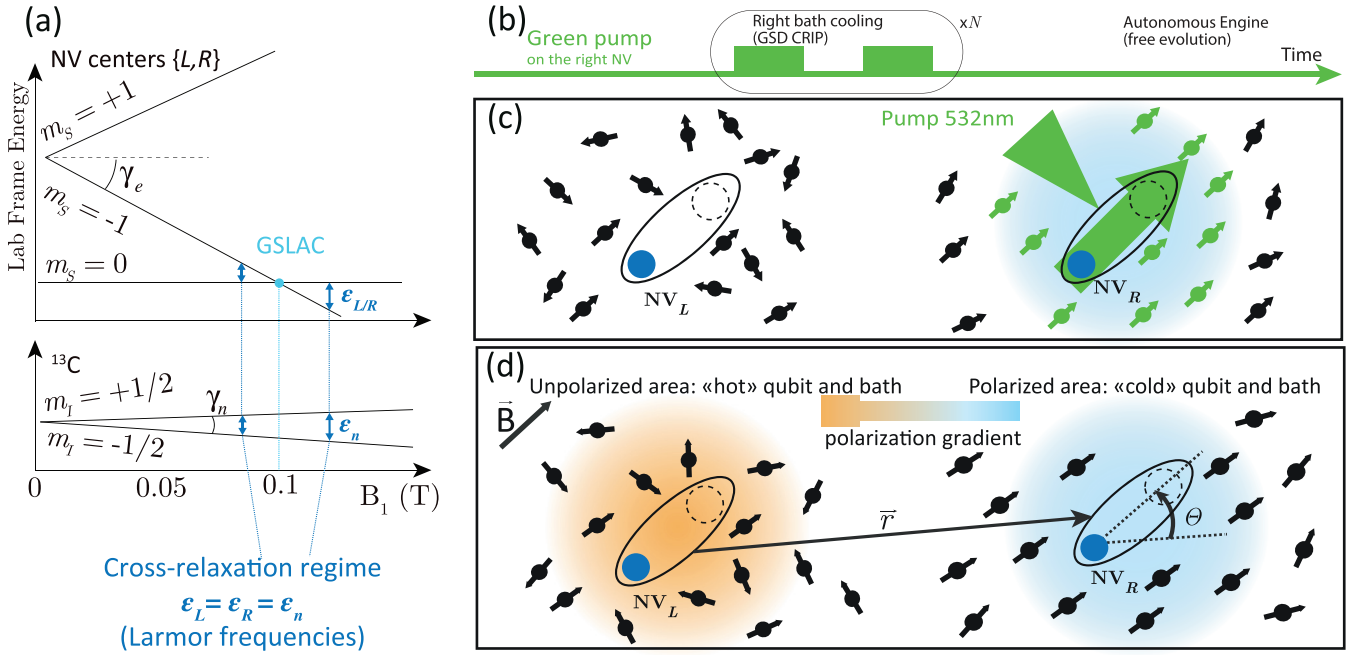

FIG. 2. Experimental configuration no. 1 corresponding to the CR regime. (a) A magnetic field is applied along the common quantization axis of the two NV centers such that they are in direct resonance with each other and with the ^{13}C. In the experimental sequence (b), the STED or the GSD superresolution method enables us to optically polarize one of the two NV centers (e.g., the right one) selectively, allowing us to apply a CRIP polarization to cool the corresponding bath (c). In a second phase (d), free of any external fields, microwaves or optical, the CR regime induces the flip-flop interaction Hamiltonian between the two NV centers and optimizes the relaxation interaction with their respective bath to realize the engine for entanglement generation.

discussed in the next section, the HH regime allows for the implementation of the interqubit interaction Hamiltonian. Let us mention that other sequences allow for the HH regime, for instance the PulsePol sequence used in [31,42].

D. Role of the hyperfine coupling term H_N and choice of the nitrogen isotope

We now discuss the additional term H_N in Eq. (4), corresponding to the hyperfine coupling with the nitrogen atoms. Within the CR regime, near GSLAC, H_N plays an important role which depends on the nitrogen isotope used in the experiment [43,44]. As shown in Ref. [39], the energy transition between states $|m_s = 0\rangle$ and $|m_s = -1\rangle$ of a ^{15}NV center comprising the nuclear doublet ^{15}N isotope cannot be lowered below 2 MHz and reach the ^{13}C nuclear transition. This makes the ^{15}NV unsuitable for configuration no. 1 in the CR regime. Instead, the nuclear triplet ^{14}N is naturally much more abundant (>99.5 %) than the other isotopes. Importantly, it has been demonstrated to reach the cross-relaxation regime with either ^{13}C or other nuclear spins of higher gyromagnetic ratio [29,40]. This makes ^{14}N suitable for both configurations no. 1 and no. 2, i.e., for the CR and HH regimes. This is why we foresee it as the most natural choice to realize the surrounding nuclear spin environments for the electron spins. Finally, it is now well established that the nuclear spin I_n of the ^{14}N atom can be initialized to its noninteracting $|m_I = 0\rangle$ state [44] in a durable manner [45,46]. It renders the role of H_N negligible both for the CR and the HH regimes (no evolution due to H_N).

E. Interqubit dipole-dipole interaction

In the laboratory frame, the electronic spins of two NV centers interact naturally through a dipole-dipole interaction, whose strength depends on the electromagnetic gyromagnetic ratio γ_e of each NV center and on the relative distance between them characterized by the vector $\vec{r} = r\hat{e}_R$ below. Within the secular approximation (valid at high magnetic field), the dipole-dipole interaction Hamiltonian takes the form [47–49]

$$H_{LR} = \frac{\mu_0 \gamma_e \gamma_e \hbar}{4\pi r^3}(1 - 3\cos^2\theta)\left(S_L^z S_R^z - \frac{1}{4}(S_L^+ S_R^- + S_R^+ S_L^-)\right), \tag{10}$$

where the first two terms correspond to the terms A and B of the dipolar alphabet of the dipole interaction Hamiltonian. Let us note that, for clarity, we have omitted the tensor product in the above equation compared to Eq. (1). In the literature, the case of two off-resonant nuclear spins is typically discussed such that the second term is neglected. In Eq. (10), one notes that the second interaction term realizes the flip-flop interaction required by Eq. (1) with the coupling constant g set by

$$|g| = \frac{\mu_0 \gamma_e^2 \hbar}{4\pi r^3}\frac{1 - 3\cos^2\theta}{4}. \tag{11}$$

The angle θ denotes the angle between the orientation NV-center axis and the direction of $B_\parallel$ (B_{CR}). Importantly, it was shown in Ref. [50] that the average interaction Hamiltonian in the rotating frame of the HH regime also takes the form of Eq. (10) with the desired flip-flop term. Some additional constant factors may be present, depending on the

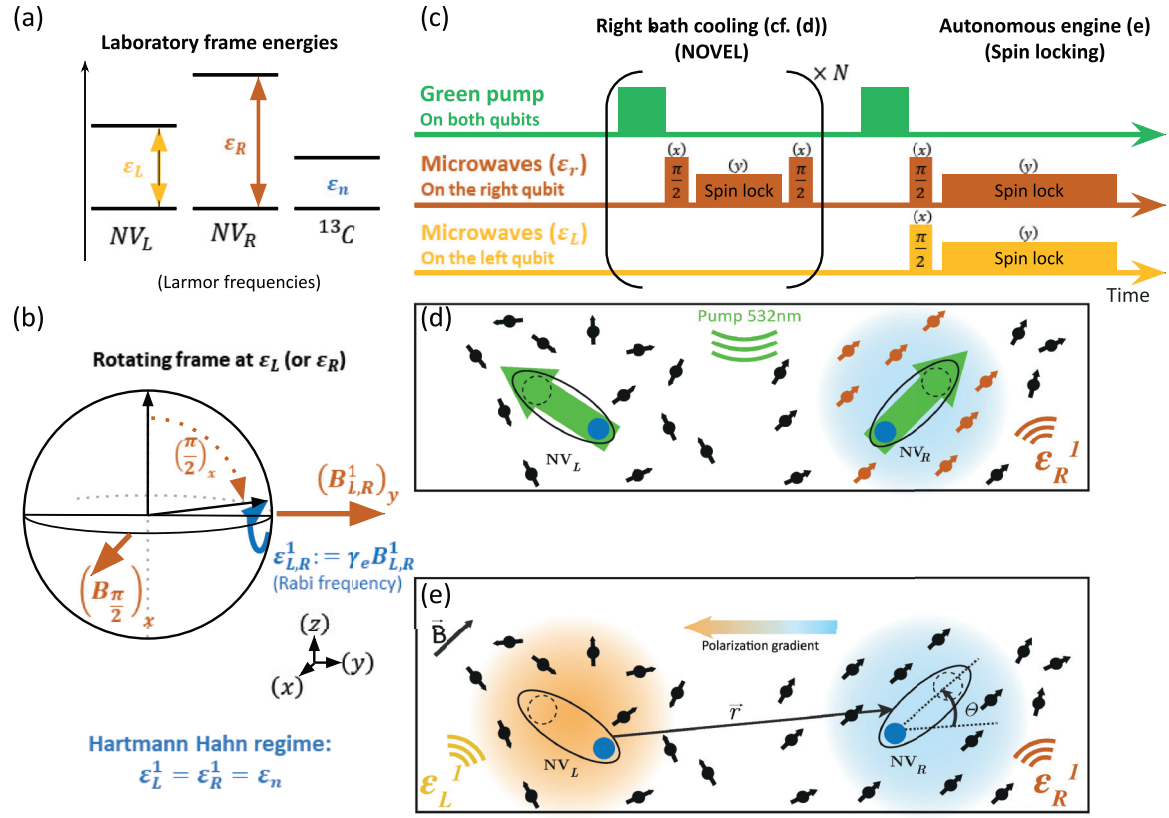

FIG. 3. Experimental configuration no. 2 corresponding to the HH regime. (a) In the HH regime, the two NV centers can have different orientations and energies. (b) The desired interqubit and qubit-bath flip-flop interactions are set through the NOVEL polarization sequence in which a laser pulse followed by a $\frac{\pi}{2}$ along the axis (x) prepares the NV center in a superposition state along (y). A magnetic field $B^1_{L,R}$ is then applied in the rotating frame along (y) to "spin-lock" the NV center, and it generates a dressed state with the desired energy. In the experimental sequence (c), the first phase (d) consists in applying the NOVEL sequence repeatedly over only one of the two NV centers (e.g., R) to cool the corresponding ^{13}C bath. In a second phase (e), the NOVEL sequence is applied on both NV centers simultaneously to turn the quantum engine on.

experimental parameters. Based on this work, it is valid to consider the Hamiltonian in Eq. (10) both for the CR and HH regimes without loss of generality.

Let us mention that the contribution of the $S^z_L S^z_R$ term only plays a role for a certain class of initial states, i.e., those that are not described by an X-shaped density operator. The predictions we make in the following sections are done considering relevant experimental initial states, which are all of an X-shape. For other initial states, this term will induce additional nonzero off-diagonal terms in the transient regime, but will not affect the steady state. We can therefore neglect this term without loss of generality for this proposal.

In both CR and HH regimes, for a successful realization of a NV-based entanglement engine, the interaction strength g must be within the right energy range with respect to bare energies of the NV centers and relaxation rates $\Gamma_{\mathrm{CR,\,HH}}$ with the surrounding ^{13}C (discussed just below), $\Gamma_{\mathrm{CR,\,HH}} \leqslant g \ll \varepsilon$. The interaction strength g depends directly on the distance between the two NV centers ($g \propto 1/r^3$). In recent years, stochastic implementation of pairs [51–53] and triplets [54] of NV centers has been achieved in experiments. The implantation energy determines the final depth and straggling [55] of the nitrogen atoms in the diamond, and therefore the expected distance that separates them. Based on magnetic spectroscopy measurements, coupling strengths ranging from a few kHz, as limited by decoherence, up to the record of 3.9 MHz reported in Ref. [52] have been demonstrated, falling well into the above range. The main experimental values of the parameters of the model that correspond to the discussions in the present and following sections are summarized in Table I.

We now discuss environment engineering and relaxation energy scales.

IV. SYSTEM-ENVIRONMENT INTERACTION

In this section, we first discuss the role of different environments for an NV center, and then we propose a scheme to engineer an out-of-equilibrium situation between two NV centers, which is required for entanglement generation.

A. Dipolar interaction

A key advantage of the NV-center platform is the excellent decoupling of NV centers from lattice phonons [56], with a room-temperature spin-lattice relaxation rate as low as a few hundred Hertz. As a consequence, quantum coherence properties of NV centers are mainly limited by surrounding magnetic impurities ^{13}C in our case [18,20,57,58].

TABLE I. Dynamical nuclear polarization parameters for different nuclear spins and concentration. Missing values are either not applicable or not available from the literature.

Nuclear bath			^{13}C 1.1 %	^{13}C 3–100 %	^{1}H biphenyl	^{1}H Al2O3	^{19}F Al2O3
Concentration	n_n	($n^{-1}\,m^3$)	1.9	5.1–170	41		
	σ_n	($n^{-1}\,m^2$)				$\gg$3	3 [67]
Polarization radius	R_M	(nm)	1.33	1.33			
NV center depth	d_{NV}	(nm)			6	10	10
Number of nuclei			20	$20 \times \frac{n_c}{n_c^0}$			
Polarization rate	R	(Hz)	9000	9000	7500	375	154
Maximal polarization	$p_{\max}$	(%)	>99	>99	few %	%	0.3
Diffusion constant	D	($nm^2\,s^{-1}$)	7 [66]	Eq. (24)	571	700	700
Gyromagnetic ratio	γ_n	($MHz\,T^{-1}$)	10.7	10.7	42.6	42.6	40.0
Qubit energy	$\varepsilon_{\mathrm{L,R}}$	(MHz)	1.1	1.1	4.4	4.4	4.1
Qubit/bath coupling	$\Gamma^{(i)}_{1,\mathrm{CR}}$	(kHz)	250	Eq. (18)	few 1000	few 1000	few 1000
Decoherence	$\Gamma^{(i)}_{2}$	(kHz)	1.5 [57]	Eq. (19)	$(4.5–14) \times 10^3$	few 100	
Spin-lattice relaxation	$\Gamma^{(i)}_{1,\mathrm{SL}}$	(Hz)	150	150	150	150	150
Reference			[29,32]		[31]	[32]	[32]

The interactions between a NV center's electron spin α and the jth $^{13}C'$s nuclear spin is again described by the dipole-dipole Hamiltonian. Within the secular approximation, under resonant conditions discussed in the previous section, the electron spin α (with a gyromagnetic ratio γ_e) interacts with N ^{13}C nuclear spins (with a gyromagnetic ratio γ_n) with the Hamiltonian $H_{T,\alpha}$,

$$H_{T,\alpha} = \sum_{j=1}^{N} \frac{\mu_0 \gamma_e \gamma_n \hbar}{4\pi {r_{\alpha j}}^3}(1 - 3\cos^2\theta_{\alpha j}) \times \left(S_\alpha^z I_j^z - \frac{1}{4}(S_\alpha^+ I_j^- + I_j^+ S_\alpha^-) \right). \quad (12)$$

Here, $\vec{S}_{\mathrm{L,R}}$ and $\vec{I}_j$ denote the spin and nuclear operators, respectively. The term $S_\alpha^z I_j^z$ will lead to pure dephasing via the rate $\Gamma_{2,\varphi}$ of the electron spin of the NV centers, while the tunneling (flip-flop) term is at the origin of dissipation (decoherence rate $\Gamma_{2,\mathrm{CR}}$ and relaxation rate $\Gamma_{1\alpha}$). In the following subsections, we discuss in further detail these rates and predicted values in the context of our proposal.

B. Relaxation in the CR regime

The effect of the ^{13}C nuclei on the relaxation of the NV center α is known to be determined by the product of the root-mean-square value of the transverse magnetic field noise, $B_{\mathrm{rms},\alpha}$, and its spectral density $S_\alpha(\varepsilon)$ [47,59],

$$\Gamma_{1,\alpha}(\varepsilon) = 3\gamma_e^2 (B_{\mathrm{rms},\alpha})^2 S_\alpha(\varepsilon). \quad (13)$$

In full generality, the spin-lattice relaxation rate Γ_{SL} needs to be added to this expression if non-negligible. Considering the contributions of all ^{13}C nuclei to be independent from each other, $(B_{\mathrm{rms},\alpha})^2$ can be obtained by summing up all the contributions squared [47],

$$(B_{\mathrm{rms},\alpha})^2 = \sum_j \left(\frac{\mu_0 \gamma_n \hbar}{4\pi} \right)^2 C_S \frac{2 + 3\sin^2\theta_{\alpha j}}{{r_{\alpha j}}^6}, \quad (14)$$

where $C_S = 1/4$ is linked to the multiplicity of the reservoir spins. The number of nuclear spins contributing to the sum over j can be estimated through the volume of influence [60,61]. Nuclear spins that are closer than a minimal radius around the NV center, $R_m \approx 0.2$ nm, as well as the ones beyond a maximal radius, $R_M \approx 1.33$ nm, are excluded. In a diamond with a natural abundance of ^{13}C of $n_C = 1.1$ %, we estimate the sum over j to comprise approximately 20 spins, which will define the environment of the electron spin of the NV center α. Assuming $r_{\alpha j} = r_\alpha$ and the same orientation of the nuclear spins with respect to the quantization axis of spin α, $\theta_{\alpha j} = \theta_\alpha$, Eq. (14) can then be written as

$$(B_{\mathrm{rms},\alpha})^2 = C_S \left(\frac{\mu_0 \gamma_n \hbar}{4\pi} \right)^2 \iiint_{r>R_m} \frac{2 + 3\sin^2\theta_\alpha}{r^6} n_C dV, = C_S \left(\frac{\mu_0 \gamma_n \hbar}{4\pi} \right)^2 \frac{7\pi}{2{R_m}^3} n_C, \quad (15)$$

where n_C is the average ^{13}C density, or its natural abundance.

The spectral density $S_\alpha(\varepsilon)$ is approximated by a Lorentzian, centered on the nuclear spin energy $\varepsilon_n = \gamma_n B_\parallel$, and whose linewidth is limited by the NV center decoherence $\Gamma_{2,\alpha}$ [62,63],

$$S_\alpha(\varepsilon) = \frac{1}{\Gamma_{2,\alpha}} \times \frac{1}{1 + (\varepsilon - \varepsilon_n)^2 / \Gamma_{2,\alpha}^2}. \quad (16)$$

In the most common off-resonance case ($\varepsilon_\alpha \gg \varepsilon_n$), the spectral density vanishes such that the nuclear-spin-induced relaxation remains small with respect to the spin lattice one.

Instead, under the cross-relaxation condition that applies here, ($\varepsilon_{\mathrm{L,R}} = \varepsilon_n$), the maximal relaxation rate, hereby called the cross-relaxation rate, has the form

$$\Gamma_{1,\alpha} = \frac{3\gamma_e^2 \left(B_{\mathrm{rms}}^\alpha\right)^2}{\Gamma_{2,\alpha}}. \quad (17)$$

It has been measured up to $\Gamma_{1,\alpha} = 250$ kHz in a diamond with a natural concentration of ^{13}C [29], three orders of

magnitude larger than the spin-lattice relaxation rate 200 Hz in the same sample.

For our proposal, considering the natural abundance n_C, the cross-relaxation bare rate Γ_α in Eq. (3) will be taken to be

$$\Gamma_1 \equiv \Gamma_{1,\alpha}(\%(^{13}\mathrm{C})) = \frac{\%(^{13}\mathrm{C})}{1.1\,\%} \times 250\ \mathrm{kHz}. \tag{18}$$

In a similar sample diamond, the decoherence rate is measured to be of the order of 1.5 kHz [57], with a linear increase with n_C:

$$\Gamma_{2,\alpha}(\%(^{13}\mathrm{C})) = \frac{\%(^{13}\mathrm{C})}{1.1\,\%} \times 1.5\,\mathrm{kHz}. \tag{19}$$

This remains two orders of magnitude lower than the relaxation rate. In the cross-relaxation regime, the dynamics of the NV centers' electron spins can therefore be modeled by the purely dissipative cross-relaxation process, for which Eq. (2) should be valid. In the following, we consider the same bare rates for the electron spins coupled to their respective nuclear spin baths, $\Gamma_\mathrm{L} = \Gamma_\mathrm{R} = \Gamma_1$, given by Eq. (18).

C. Relaxation in the HH regime

As introduced in Sec. III E, low-field DNP methods allow us to set a flip-flop Hamiltonian between spins of different energy. When combined with optical pumping repolarizing the NV centers, this is commonly used to hyperpolarize the surrounding nuclear spin bath [see also Fig. 3(c) and Sec. V]. In addition, it symmetrically maximizes the coupling for the (cross)-relaxation process [30–32] [Fig. 3(d)], and this is commonly used to probe the polarization transfer to the nuclear spins, similar to what is done in the CR regime [40]. Hence, the rates derived for the CR regime correspond to the symmetrized rates in the HH regime, and we will consider them for our predictions.

V. THERMALLY BIASED ENVIRONMENTS

In this section, we explain how to engineer two artificial thermal environments made of ^{13}C nuclear spins, biased in temperature. In an NV-center platform, this is made possible due to the NV centers being naturally decoupled from the phonons [56], allowing us to not be subject to the excellent thermal conduction properties of the diamond. Here, we realize an effective temperature difference between two ensembles of nuclear spins through DNP techniques in the CR and HH regimes. We predict that these regimes will enable a long-lasting out-of-equilibrium situation within the context of this proposal. The main steps are shown in Figs. 2 and 3 and discussed below.

A. Polarization

For the nuclear spins with energy ε_n, at a position $\vec{r}$ and time t, it is possible to estimate their polarization $p = p_\downarrow - p_\uparrow$ by assuming a Boltzmann distribution for each of the nuclear spin states $p_\downarrow = 1/(e^{-\varepsilon_n/(k_B T)} + 1)$ and $p_\uparrow = 1 - p_\downarrow$,

$$p = p_\downarrow - p_\uparrow = \frac{1 - e^{-\varepsilon_n/k_b T}}{1 + e^{-\varepsilon_n/k_b T}}. \tag{20}$$

At room temperature, with $\varepsilon_n = 1.1$ MHz and $B_\mathrm{CR} = 102$ mT, we obtain $p \approx 10^{-7}$, corresponding to a situation without any effective temperature gradient. In recent years, several methods have been proposed and experimentally demonstrated to lower or increase the polarization of nuclear spins by transferring the optically induced polarization of an electron spin in their vicinity. These methods rely on DNP, in various regimes, including CR and HH regimes. The principle goes as follows.

The NV centers' electron spin can be polarized optically to its $|m_S = 0\rangle$ state [12] via its spin-selective nonradiative decay path (see Fig. 1). DNP uses this polarization as a source to transfer it to the surrounding nuclear spins. This can be achieved if a resonant condition between the electron spin and the nuclear spins is satisfied, which can be done in the CR and HH regimes discussed in the previous sections. As shown in Ref. [61], the NV centers have an influence on a specific volume of influence, which depends in general on the chosen DNP method (and consequently on the regime). In our case, the same DNP regime is used for both the cooling and for realizing the quantum engine [see Figs. 2(c) and 2(d) and Figs. 3(d) and 3(e)]. This implies that the polarization efficiencies obtained in previous works are also valid in our scheme.

Consequently, the above sequences are suitable both to cool down nuclear spins within the volume of influence of a given NV center, and to realize the adequate thermal baths with distinct effective temperatures. We provide the details for each regime below.

B. Cross-relaxation-induced polarization

In the CR regime, a strong magnetic field is required to align the NV center axes (see Sec. III A). With this experimental condition, the so-called CRIP methods (cross-relaxation induced polarization) have the advantage of not requiring any driving microwaves [see Fig. 2(c)]. In Ref. [29], a polarization efficiency above 99 % for either ^{13}C or ^{1}H bath have been evidenced. However, it remains a challenge to apply CRIP to only one of the NV centers. Indeed, as shown in Sec. VI and Fig. 4(a), the optimal coupling efficiency for a diamond with a natural ^{13}C concentration of about 50 kHz corresponds to a distance of about 10 nm. The constraint imposed by this very short distance can be slightly reduced by considering smaller qubit-bath coupling strength (see the discussion in Sec. IV A, $\Gamma_{\mathrm{CR,\,HH}} \leqslant g \ll \varepsilon$). This could be achieved either by introducing a small amount of energy detuning between the two NV centers, see Eq. (16) (but this will decrease the amount of entanglement in the steady state), or by utilizing a diamond with a lower ^{13}C concentration [see Eq. (18)].

In any case, microscopic superresolution techniques will be necessary in the CR regime to reach these distances of a few nm. Here we propose to use either the GSD [15] technique or the STED [16] one earlier [see Fig. 2(b)]. In the case of GSD, the pumping beam (green) is patterned to have a central dark spot on the focus plane (see Fig. 1). The NV center within the dark spot is therefore not optically pumped while the other is. In the case of STED, a similarly patterned depletion beam [16] is added to a conventional green pump. The NV center placed in the dark center of that red beam is pumped normally, while

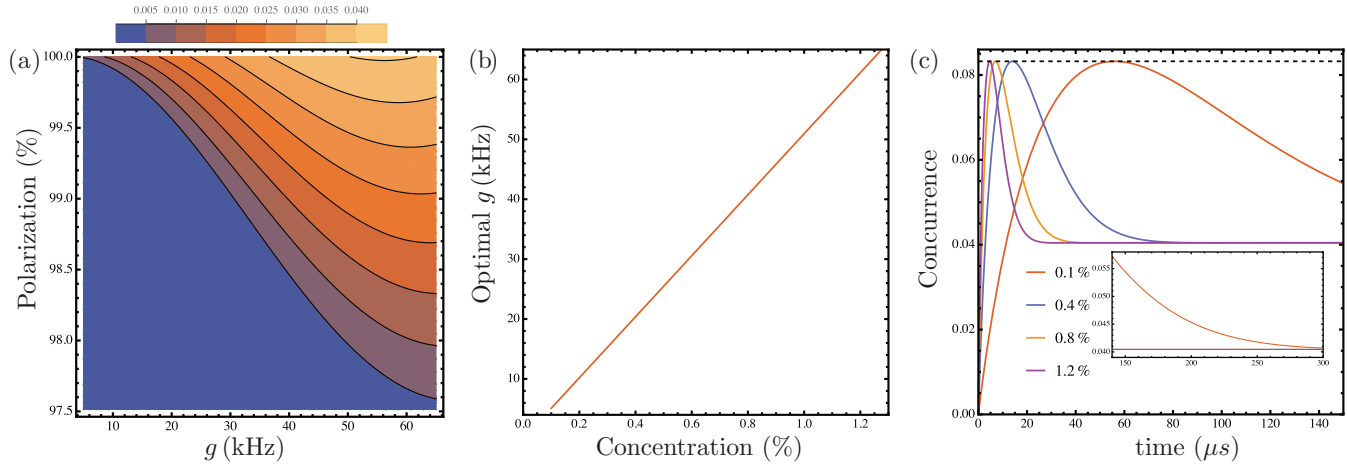

FIG. 4. Entanglement predicted between the two NV centers. (a) Contour plot showing the concurrence as a function of the polarization % and the interqubit coupling, g. The other parameters are $\varepsilon = 1.1\,\mathrm{MHz}$, $T_h = 1\,\mathrm{GHz}$, and natural concentration of $^{13}\mathrm{C} = 1.1\,\%$. (b) The optimal values (i.e., optimized to maximize the steady-state concurrence) of interqubit coupling for given $^{13}\mathrm{C}$ concentrations. (c) Transient behavior of concurrence for four different values of concentration and the corresponding optimal value of interqubit coupling. The other parameters are $\varepsilon = 1.1\,\mathrm{MHz}$, $T_h = 1\,\mathrm{GHz}$, and 100 % polarization of $^{13}\mathrm{C}$ constituting the cold reservoir. The initial state is chosen to be a tensor product of thermal states at the reservoir temperatures (i.e., with $n_F^c = 0$ and $n_F^h \approx 1/2$). The couplings are such that $g < 70\,\mathrm{kHz} < \Gamma_{1,\mathrm{CR}}^{(i)} = 250\,\mathrm{kHz}$, which fits the chosen master equation regime.

the excited state of the other NV center is depleted such that its spin-nonconservative decay path is impeached. In either case, only one of the two NV centers can be regularly pumped and act as a local source of polarization for a DNP protocol.

Importantly for this work, Ref. [17] reported STED on NV centers with a point-spread function of width below 6 nm with an incoming beam of a few hundred milliwatts. Although certainly challenging experimentally, this appears to be compatible with the predicted optimal distance of a natural $^{13}\mathrm{C}$ concentration without detuning the NV centers in the context of our proposal.

C. Polarization in the HH regime

In the HH regime, the two NV centers may have different Larmor energies and can therefore be selected through their ODMR spectrum [64], relaxing the need of superresolution methods [see Figs. 3(c) and 3(d)]. This selective cooling process therefore appears more direct experimentally.

D. Effective coupling rates to out-of-equilibrium thermal baths

With the above experimental considerations about the configurations in the CR and HH regimes, we are now able to connect experimental parameters discussed in the previous sections with the theoretical model. To summarize, in our proposal the hot bath is realized by considering the nuclear spins surrounding the left NV center (for instance), the effective hot temperature being the room temperature corresponding to a polarization close to 0. The cold bath will be realized through DNP and selective cooling as discussed above and shown in Figs. 2(d) and 3(d). The predicted effective cold temperature is estimated through the achieved polarization in the range 97–100 %. With these experimental achievements, the rates entering the Lindblad master equation (2) for the left (hot) and right (cold) baths can be identified as

$$\gamma_{\mathrm{L}}^{+} = \gamma_{\mathrm{L}}^{-} = \frac{1}{2}\,\Gamma_1, \tag{21}$$

$$\gamma_{\mathrm{R}}^{-} = \frac{1+p_{\mathrm{R}}}{2}\,\Gamma_1 = [1 - n_F(\varepsilon, T_{\mathrm{R}})]\Gamma_1, \tag{22}$$

$$\gamma_{\mathrm{R}}^{+} = \frac{1-p_{\mathrm{R}}}{2}\,\Gamma_1 = n_F(\varepsilon, T_{\mathrm{R}})\Gamma_1, \tag{23}$$

with $p_{\mathrm{R}} \in [0.97, 1]$ and Γ_1 given by Eq. (18). Before discussing the numerical predictions for this NV-center-based entanglement engine, we comment on spin diffusion and spin-lattice relaxation that would, in general, affect DNP protocols.

E. Spin diffusion

In general, spin polarization in DNP protocols may also happen through spin diffusion, as spins interact directly through the dipole-dipole interaction Hamiltonian [similar to Eq. (10)].

In a 100 % enriched diamond, the spin diffusion constant can be calculated directly, $D_n(100\,\%) = 6.5\,\mathrm{nm^2\,s^{-1}}$. It has a square-root dependence on n_C [65]. For our proposal, we estimate it to be

$$D_C(\%(^{13}C)) = \sqrt{\frac{\%(^{13}C)}{100\,\%}} \times 6.5\,\mathrm{nm^2\,s^{-1}}. \tag{24}$$

This is also consistent with the experimental value of $6.5\,\mathrm{nm^2\,s^{-1}}$ obtained in [60] for a diamond with $^{13}\mathrm{C}$ in natural abundance. Another indirect experimental estimation gives a diffusion constant higher by one order of magnitude [66].

However, this is related to a diamond being with additional nitrogen impurities, which can mediate the spin diffusion. Accounting for spin diffusion, the polarization of a given bath is expected to propagate over a distance of $d = 20\,\text{nm}$ in $\approx \frac{d^2}{D_C} = 1\,\text{min}$. This timescale is orders of magnitude higher than the other timescales involved in this proposal, which are of the order of tens of microseconds [see Fig. 4(c) and previous discussions]. We therefore predict this spin diffusion to be negligible in the realization of an entanglement engine.

In the final section, we present numerical estimations for the concurrence, a measure for entanglement. We investigate it as a function of relevant parameters of the proposal, the polarization of the nuclear spin baths, the concentration of ^{13}C, and the coupling g between the NV centers, which is determined by the distance between them. These predictions show that the above experimental methods and associated configurations can generate a long-lasting out-of-equilibrium thermal situation suitable for the quantum engine to function.

VI. ENTANGLEMENT GENERATION

Having discussed all of the relevant factors that determine the quantum evolution of the NV centers in our scheme, we now proceed to discuss the dynamics. For this purpose, we take the master-equation approach described in Sec. I. Analytical results on both steady-state [6] and transient regimes [68] have been previously discussed for the system. Here, we focus on numerically demonstrating the generation of entanglement considering values for the parameters that correspond to the techniques and regimes described in the previous sections.

In Fig. 4(a), we show the steady-state concurrence [69] as a function of polarization and coupling between the NV centers for natural concentrations of ^{13}C . We find that there is a large range of experimental parameters for which the qubits become entangled in the steady state. Specifically, the higher the polarization (i.e., the lower the effective temperature of the "cold" reservoir), and the larger the coupling between them (i.e., the smaller the distance between them), the higher the steady-state entanglement. The entanglement is larger with increasing temperature gradient, but the maximum takes place at an intermediate interqubit coupling. The parameter range where entanglement is nonzero can be obtained exactly via the critical heat current introduced in [68].

In general, entanglement may appear in the transient dynamics and may disappear completely at long times. Furthermore, depending on the timescale of the dynamics of the machine, it may be more experimentally feasible to look at short or intermediate times to detect entanglement. Importantly, the entanglement at an intermediate time may be much larger than at long times. It is therefore also important to investigate entanglement production in the transient regime. In Fig. 4(c), the goal is to see how much entanglement can be created at intermediate times for different concentrations of ^{13}C in the diamond sample. In Fig. 4(b), for a given concentration, we plot the optimal value of g (i.e., the value that maximizes transient concurrence). In Fig. 4(c), we use this value of g to plot the concurrence as a function of time. We find that for any given concentration, there is a g, such that concurrence can be maximized to the same value in the transient state, which is more than double the steady-state concurrence. Since g is one of the factors that determines the timescale of the dynamics, this maximum, however, happens at different points in time. Interestingly, in the steady state, all curves approach the same value of concurrence (see the inset).

VII. CONCLUSION

In this work, we have proposed an experimental setup to realize a two-qubit entanglement engine on an NV-center platform. We discuss the implementation of two interacting qubits, as well as the realization of two independent nuclear spin baths characterized by different temperatures. This temperature gradient is realized effectively through a polarization gradient created using DNP. We detail two relevant experimental configurations either corresponding to the CR regime or to the HH one. Their distinct advantages are discussed in relation to each experimental aspect that is to be implemented. It is interesting to note that certain DNP protocols can also engineer effective baths at negative temperature [31,32], corresponding to spin baths polarized in their "up" state. From a thermodynamic point of view, this constitutes an interesting resource, already discussed in a few works in the context of quantum thermal machines [10,70,71].

A key requirement of a two-qubit engine is to maintain a long-lasting out-of-equilibrium situation. In schemes involving local interactions, this appears particularly difficult. It is indeed required to avoid any direct coupling between the two thermal reservoirs, at a similar distance to one another compared to the one between qubits, while keeping dominating qubits/qubit and qubit/bath couplings with a similar order of magnitude. In our scheme, this is made possible by exploiting the large difference between the gyromagnetic moments of, on one side, the nuclear spins for the baths, and on the other side the electron spins for the two interacting qubits. For instance, with the alternative of considering baths made of electron spins, all interaction strengths would be set by the gyromagnetic moments of electron spins, preventing the realization of two independent reservoirs interacting distinctively with each NV center.

As a possible alternative, one may consider different nuclear spins. For instance, in Refs. [31,32], local efficient polarization of surface nuclear spins ^{19}F or ^{1}H has been demonstrated. The relevant references and parameters to investigate such configurations together with alternative ^{13}C volume concentrations are provided in Table I. In those cases, one could take advantage of the potentially shorter distance between nuclei to strengthen the thermal reservoir approximation by involving more of them in each bath, thus enabling interactions between them. The qubit/bath coupling could then be set by the NV centers' depths. In such cases, however, the spin diffusion to be considered may no longer be negligible and would require a proper modeling. Such alternatives may constitute interesting schemes to be investigated both theoretically and experimentally.

ACKNOWLEDGMENTS

The authors thank Christophe Galland and Jonatan Bohr Brask for discussions at an early stage of this work. All of

the authors acknowledge support from the Swiss National Science Foundation—G.H. and S.Kh. through the Starting Grant PRIMA No. 179748, and M.C. and S.Ku. through the Ambizione Grant No. 185824.

[1] S. Bravyi, O. Dial, J. M. Gambetta, D. Gil, and Z. Nazario, The future of quantum computing with superconducting qubits, J. Appl. Phys. **132**, 160902 (2022).

[2] C. D. Bruzewicz, J. Chiaverini, R. McConnell, and J. M. Sage, Trapped-ion quantum computing: Progress and challenges, Appl. Phys. Rev. **6**, 021314 (2019).

[3] J. Bohr Brask, G. Haack, N. Brunner, and M. Huber, Autonomous quantum thermal machine for generating steady-state entanglement, New J. Phys. **17**, 113029 (2015).

[4] A. Tavakoli, G. Haack, M. Huber, N. Brunner, and J. B. Brask, Heralded generation of maximal entanglement in any dimension via incoherent coupling to thermal baths, Quantum **2**, 73 (2018).

[5] A. Tavakoli, G. Haack, N. Brunner, and J. B. Brask, Autonomous multipartite entanglement engines, Phys. Rev. A **101**, 012315 (2020).

[6] S. Khandelwal, N. Palazzo, N. Brunner, and G. Haack, Critical heat current for operating an entanglement engine, New J. Phys. **22**, 073039 (2020).

[7] M. Aguilar, N. Freitas, and J. P. Paz, Entanglement generation in quantum thermal machines, Phys. Rev. A **102**, 062422 (2020).

[8] A. Das, A. A. Khan, S. D. Mishra, P. Solanki, B. De, B. Muralidharan, and S. Vinjanampathy, Steady-state tunable entanglement thermal machine using quantum dots, Quantum Sci. Technol. **7**, 045034 (2022).

[9] M. T. Naseem and Ö. E. Müstecaplıoğlu, Engineering entanglement between resonators by hot environment, Quantum Sci. Technol. **7**, 045012 (2022).

[10] J. B. Brask, F. Clivaz, G. Haack, and A. Tavakoli, Operational nonclassicality in minimal autonomous thermal machines, Quantum **6**, 672 (2022).

[11] K. Prech, P. Johansson, E. Nyholm, G. T. Landi, C. Verdozzi, P. Samuelsson, and P. P. Potts, Entanglement and thermokinetic uncertainty relations in coherent mesoscopic transport, Phys. Rev. Res. **5**, 023155 (2023).

[12] A. Gruber, A. Dräbenstedt, C. Tietz, L. Fleury, J. Wrachtrup, and C. V. Borczyskowski, Scanning confocal optical microscopy and magnetic resonance on single defect centers, Science **276**, 2012 (1997).

[13] D. Suter, Optical detection of magnetic resonance, Magn. Reson. **1**, 115 (2020).

[14] H. Babashah, H. Shirzad, E. Losero, V. Goblot, C. Galland, and M. Chipaux, Optically detected magnetic resonance with an open source platform, SciPost Phys. Core **6**, 065 (2023).

[15] J. Storterboom, M. Barbiero, S. Castelletto, and M. Gu, Ground-state depletion nanoscopy of nitrogen-vacancy centres in nanodiamonds, Nanoscale Res. Lett. **16**, 44 (2021).

[16] S. Arroyo-Camejo, M.-P. Adam, M. Besbes, J.-P. Hugonin, V. Jacques, J.-J. Greffet, J.-F. Roch, S. W. Hell, and F. Treussart, Stimulated emission depletion microscopy resolves individual nitrogen vacancy centers in diamond nanocrystals, ACS Nano **7**, 10912 (2013).

[17] E. Rittweger, K. Y. Han, S. E. Irvine, C. Eggeling, and S. W. Hell, Sted microscopy reveals crystal colour centres with nanometric resolution, Nat. Photon. **3**, 144 (2009).

[18] G. Balasubramanian, P. Neumann, D. Twitchen, M. Markham, R. Kolesov, N. Mizuochi, J. Isoya, J. Achard, J. Beck, J. Tissler, V. Jacques, P. R. Hemmer, F. Jelezko, and J. Wrachtrup, Ultralong spin coherence time in isotopically engineered diamond, Nat. Mater. **8**, 383 (2009).

[19] L. Rondin, J.-P. Tetienne, T. Hingant, J.-F. Roch, P. Maletinsky, and V. Jacques, Magnetometry with nitrogen-vacancy defects in diamond, Rep. Prog. Phys. **77**, 056503 (2014).

[20] J. F. Barry, J. M. Schloss, E. Bauch, M. J. Turner, C. A. Hart, L. M. Pham, and R. L. Walsworth, Sensitivity optimization for NV-diamond magnetometry, Rev. Mod. Phys. **92**, 015004 (2020).

[21] B. Bürgler, T. F. Sjolander, O. Brinza, A. Tallaire, J. Achard, and P. Maletinsky, All-optical nuclear quantum sensing using nitrogen-vacancy centers in diamond, npj Quantum Inf. **9**, 56 (2023).

[22] K. O. Ho, K. C. Wong, M. Y. Leung, Y. Y. Pang, W. K. Leung, K. Y. Yip, W. Zhang, J. Xie, S. K. Goh, and S. Yang, Recent developments of quantum sensing under pressurized environment using the nitrogen vacancy (NV) center in diamond, J. Appl. Phys. **129**, 241101 (2021).

[23] G. Q. Liu, X. Feng, N. Wang, Q. Li, and R. B. Liu, Coherent quantum control of nitrogen-vacancy center spins near 1000 Kelvin, Nat. Commun. **10**, 1344 (2019).

[24] M. Chipaux, K. van der Laan, S. Hemelaar, M. Hasani, T. Zheng, and R. Schirhagl, Nanodiamonds and their applications in cells, Small **14**, 1704263 (2018).

[25] S. Pezzagna and J. Meijer, Quantum computer based on color centers in diamond, Appl. Phys. Rev. **8**, 011308 (2021).

[26] C. Bradley, S. de Bone, P. Möller, S. Baier, M. Degen, S. Loenen, H. Bartling, M. Markham, D. Twitchen, R. Hanson *et al.*, Robust quantum-network memory based on spin qubits in isotopically engineered diamond, npj Quantum Inf. **8**, 122 (2022).

[27] M. J. Degen, S. J. Loenen, H. P. Bartling, C. E. Bradley, A. L. Meinsma, M. Markham, D. J. Twitchen, and T. H. Taminiau, Entanglement of dark electron-nuclear spin defects in diamond, Nat. Commun. **12**, 3470 (2021).

[28] C. E. Bradley, J. Randall, M. H. Abobeih, R. C. Berrevoets, M. J. Degen, M. A. Bakker, M. Markham, D. J. Twitchen, and T. H. Taminiau, A ten-qubit solid-state spin register with quantum memory up to one minute, Phys. Rev. X **9**, 031045 (2019).

[29] D. A. Broadway, J.-P. Tetienne, A. Stacey, J. D. A. Wood, D. A. Simpson, L. T. Hall, and L. C. L. Hollenberg, Quantum probe hyperpolarisation of molecular nuclear spins, Nat. Commun. **9**, 1246 (2018).

[30] F. Shagieva, S. Zaiser, P. Neumann, D. B. R. Dasari, R. Stöhr, A. Denisenko, R. Reuter, C. A. Meriles, and J. Wrachtrup, Microwave-assisted cross-polarization of nuclear spin

ensembles from optically pumped nitrogen-vacancy centers in diamond, Nano Lett. **18**, 3731 (2018).

[31] A. J. Healey, L. T. Hall, G. A. L. White, T. Teraji, M.-A. Sani, F. Separovic, J.-P. Tetienne, and L. C. L. Hollenberg, Polarization transfer to external nuclear spins using ensembles of nitrogen-vacancy centers, Phys. Rev. Appl. **15**, 054052 (2021).

[32] R. Rizzato, F. Bruckmaier, K. S. Liu, S. J. Glaser, and D. B. Bucher, Polarization transfer from optically pumped ensembles of N-V centers to multinuclear spin baths, Phys. Rev. Appl. **17**, 024067 (2022).

[33] J.-P. Tetienne, L. T. Hall, A. J. Healey, G. A. L. White, M.-A. Sani, F. Separovic, and L. C. L. Hollenberg, Prospects for nuclear spin hyperpolarization of molecular samples using nitrogen-vacancy centers in diamond, Phys. Rev. B **103**, 014434 (2021).

[34] S. R. Hartmann and E. L. Hahn, Nuclear double resonance in the rotating frame, Phys. Rev. **128**, 2042 (1962).

[35] D. Heineken, K. Beyer, K. Luoma, and W. T. Strunz, Quantum-memory-enhanced dissipative entanglement creation in nonequilibrium steady states, Phys. Rev. A **104**, 052426 (2021).

[36] H. P. Breuer and F. Petruccione, *The Theory of Open Quantum Systems* (Oxford University Press, 2007), Vol. 1.

[37] X.-D. Chen, F.-W. Sun, C.-L. Zou, J.-M. Cui, L.-M. Zhou, and G.-C. Guo, Vector magnetic field sensing by a single nitrogen vacancy center in diamond, Europhys. Lett. **101**, 67003 (2013).

[38] M. Chipaux, A. Tallaire, J. Achard, S. Pezzagna, J. Meijer, V. Jacques, J.-F. Roch, and T. Debuisschert, Magnetic imaging with an ensemble of nitrogen-vacancy centers in diamond, Eur. Phys. J. D **69**, 166 (2015).

[39] D. A. Broadway, J. D. A. Wood, L. T. Hall, A. Stacey, M. Markham, D. A. Simpson, J.-P. Tetienne, and L. C. L. Hollenberg, Anticrossing spin dynamics of diamond nitrogen-vacancy centers and all-optical low-frequency magnetometry, Phys. Rev. Appl. **6**, 064001 (2016).

[40] J. D. Wood, J. P. Tetienne, D. A. Broadway, L. T. Hall, D. A. Simpson, A. Stacey, and L. C. Hollenberg, Microwave-free nuclear magnetic resonance at molecular scales, Nat. Commun. **8**, 15950 (2017).

[41] J.-P. P. Tetienne, L. Rondin, P. Spinicelli, M. Chipaux, T. Debuisschert, J.-F. F. Roch, and V. Jacques, Magnetic-field-dependent photodynamics of single NV defects in diamond: An application to qualitative all-optical magnetic imaging, New J. Phys. **14**, 103033 (2012).

[42] I. Schwartz, J. Scheuer, B. Tratzmiller, S. Müller, Q. Chen, I. Dhand, Z.-Y. Wang, C. Müller, B. Naydenov, F. Jelezko, and M. B. Plenio, Robust optical polarization of nuclear spin baths using hamiltonian engineering of nitrogen-vacancy center quantum dynamics, Sci. Adv. **4**, eaat8978 (2018).

[43] M. Auzinsh, A. Berzins, D. Budker, L. Busaite, R. Ferber, F. Gahbauer, R. Lazda, A. Wickenbrock, and H. Zheng, Hyperfine level structure in nitrogen-vacancy centers near the ground-state level anticrossing, Phys. Rev. B **100**, 075204 (2019).

[44] V. Ivády, H. Zheng, A. Wickenbrock, L. Bougas, G. Chatzidrosos, K. Nakamura, H. Sumiya, T. Ohshima, J. Isoya, D. Budker, I. A. Abrikosov, and A. Gali, Photoluminescence at the ground-state level anticrossing of the nitrogen-vacancy center in diamond: A comprehensive study, Phys. Rev. B **103**, 035307 (2021).

[45] A. Dréau, P. Spinicelli, J. R. Maze, J.-F. Roch, and V. Jacques, Single-shot readout of multiple nuclear spin qubits in diamond under ambient conditions, Phys. Rev. Lett. **110**, 060502 (2013).

[46] V. Jacques, P. Neumann, J. Beck, M. Markham, D. Twitchen, J. Meijer, F. Kaiser, G. Balasubramanian, F. Jelezko, and J. Wrachtrup, Dynamic polarization of single nuclear spins by optical pumping of nitrogen-vacancy color centers in diamond at room temperature, Phys. Rev. Lett. **102**, 057403 (2009).

[47] C. P. Slichter, *Principles of Magnetic Resonance* (Springer Science & Business Media, 2013), Vol. 1.

[48] V. I. Chizhik, Y. S. Chernyshev, A. V. Donets, V. V. Frolov, A. V. Komolkin, and M. G. Shelyapina, *Magnetic Resonance and its Applications* (Springer, 2014).

[49] E. Dikarov, O. Zgadzai, Y. Artzi, and A. Blank, Direct measurement of the flip-flop rate of electron spins in the solid state, Phys. Rev. Appl. **6**, 044001 (2016).

[50] A. Henstra and W. Wenckebach, The theory of nuclear orientation via electron spin locking (novel), Mol. Phys. **106**, 859 (2008).

[51] T. Yamamoto, C. Müller, L. P. McGuinness, T. Teraji, B. Naydenov, S. Onoda, T. Ohshima, J. Wrachtrup, F. Jelezko, and J. Isoya, Strongly coupled diamond spin qubits by molecular nitrogen implantation, Phys. Rev. B **88**, 201201(R) (2013).

[52] I. Jakobi, S. A. Momenzadeh, F. F. De Oliveira, J. Michl, F. Ziem, M. Schreck, P. Neumann, A. Denisenko, and J. Wrachtrup, Efficient creation of dipolar coupled nitrogen-vacancy spin qubits in diamond, J. Phys.: Conf. Ser. **752**, 012001 (2016).

[53] G. Zhao-Jun, C. Xiang-Dong, L. Cong-Cong, L. Shen, Z. Bo-Wen, and S. Fang-Wen, Generation of nitrogen-vacancy center pairs in bulk diamond by molecular nitrogen implantation, Chin. Phys. Lett. **33**, 026105 (2016).

[54] M. Haruyama, S. Onoda, T. Higuchi, W. Kada, A. Chiba, Y. Hirano, T. Teraji, R. Igarashi, S. Kawai, H. Kawarada, Y. Ishii, R. Fukuda, T. Tanii, J. Isoya, T. Ohshima, and O. Hanaizumi, Triple nitrogen-vacancy centre fabrication by $C_5N_4H_n$ ion implantation, Nat. Commun. **10**, 2664 (2019).

[55] S. Pezzagna, B. Naydenov, F. Jelezko, J. Wrachtrup, and J. Meijer, Creation efficiency of nitrogen-vacancy centres in diamond, New J. Phys. **12**, 065017 (2010).

[56] J. Gugler, T. Astner, A. Angerer, J. Schmiedmayer, J. Majer, and P. Mohn, *Ab initio* calculation of the spin lattice relaxation time T_1 for nitrogen-vacancy centers in diamond, Phys. Rev. B **98**, 214442 (2018).

[57] N. Mizuochi, P. Neumann, F. Rempp, J. Beck, V. Jacques, P. Siyushev, K. Nakamura, D. Twitchen, H. Watanabe, S. Yamasaki, F. Jelezko, and J. Wrachtrup, Coherence of single spins coupled to a nuclear spin bath of varying density, Phys. Rev. B **80**, 041201(R) (2009).

[58] N. Bar-Gill, L. M. Pham, A. Jarmola, D. Budker, and R. L. Walsworth, Solid-state electronic spin coherence time approaching one second, Nat. Commun. **4**, 1743 (2013).

[59] A. Sigaeva, H. Shirzad, F. P. Martinez, A. C. Nusantara, N. Mougios, M. Chipaux, and R. Schirhagl, Diamond-based nanoscale quantum relaxometry for sensing free radical production in cells, Small **18**, 2105750 (2022).

[60] C. J. Terblanche, E. C. Reynhardt, and J. A. Van Wyk, ^{13}C spin-lattice relaxation in natural diamond: Zeeman relaxation at 4.7 T and 300 K due to fixed paramagnetic nitrogen defects, Solid State Nucl. Magn. Reson. **20**, 1 (2001).

[61] L. T. Hall, D. A. Broadway, A. Stacey, D. A. Simpson, J. P. Tetienne, and L. C. L. Hollenberg, Maximising dynamic nuclear polarisation via selective hyperfine tuning, arXiv:2012.12508.

[62] J. D. A. Wood, D. A. Broadway, L. T. Hall, A. Stacey, D. A. Simpson, J.-P. Tetienne, and L. C. L. Hollenberg, Wide-band nanoscale magnetic resonance spectroscopy using quantum relaxation of a single spin in diamond, Phys. Rev. B **94**, 155402 (2016).

[63] L. T. Hall, J. H. Cole, and L. C. L. Hollenberg, Analytic solutions to the central-spin problem for nitrogen-vacancy centers in diamond, Phys. Rev. B **90**, 075201 (2014).

[64] E. Bersin, M. Walsh, S. L. Mouradian, M. E. Trusheim, T. Schröder, and D. Englund, Individual control and readout of qubits in a sub-diffraction volume, npj Quantum Inf. **5**, 38 (2019).

[65] A. J. Parker, K. Jeong, C. E. Avalos, B. J. Hausmann, C. C. Vassiliou, A. Pines, and J. P. King, Optically pumped dynamic nuclear hyperpolarization in ^{13}C-enriched diamond, Phys. Rev. B **100**, 041203(R) (2019).

[66] A. Ajoy, B. Safvati, R. Nazaryan, J. T. Oon, B. Han, P. Raghavan, R. Nirodi, A. Aguilar, K. Liu, X. Cai, X. Lv, E. Druga, C. Ramanathan, J. A. Reimer, C. A. Meriles, D. Suter, and A. Pines, Hyperpolarized relaxometry based nuclear T_1 noise spectroscopy in diamond, Nat. Commun. **10**, 5160 (2019).

[67] K. S. Liu, A. Henning, M. W. Heindl, R. D. Allert, J. D. Bartl, I. D. Sharp, R. Rizzato, and D. B. Bucher, Surface nmr using quantum sensors in diamond, Proc. Natl. Acad. Sci. USA **119**, e2111607119 (2022).

[68] S. Khandelwal, N. Brunner, and G. Haack, Signatures of Liouvillian exceptional points in a quantum thermal machine, PRX Quantum **2**, 040346 (2021).

[69] W. K. Wootters, Entanglement of formation of an arbitrary state of two qubits, Phys. Rev. Lett. **80**, 2245 (1998).

[70] R. J. de Assis, T. M. de Mendonça, C. J. Villas-Boas, A. M. de Souza, R. S. Sarthour, I. S. Oliveira, and N. G. de Almeida, Efficiency of a quantum otto heat engine operating under a reservoir at effective negative temperatures, Phys. Rev. Lett. **122**, 240602 (2019).

[71] J. Nettersheim, S. Burgardt, Q. Bouton, D. Adam, E. Lutz, and A. Widera, Power of a quasispin quantum otto engine at negative effective spin temperature, PRX Quantum **3**, 040334 (2022).